PS Interpreting Permeability from Mercury Injection Capillary Pressure Data*

Alton A. Brown[1]

Search and Discovery Article #41660 (2015)**
Posted August 17, 2015

*Adapted from poster presentation given at AAPG 2015 Annual Convention and Exhibition, Denver, Colorado, May 31 – June 3, 2015

[1]Consultant, Richardson, TX, USA (altonabrown@yahoo.com)

Abstract

Laminar flow theory predicts a strong correlation between permeability and pore-throat distribution as revealed by Mercury Injection Capillary Pressure (MICP) data. Previous studies have developed relationships between MICP data and permeability; however, the permeabilities predicted by different methods can differ substantially from the measured permeabilities and from each other, especially in low permeability samples of interest for unconventional reservoirs. The purposes of this study are to evaluate why there is such large scatter, identify algorithms that best predict permeability over a wide range of permeabilities, and evaluate what type of permeability is actually measured by MICP data. Precision of permeability predictions is low due to insufficient MICP pressure measurements, assumption of MICP curve shape, permeability anisotropy of geological samples, and low precision and accuracy of permeability measurement of tight rocks. Four methods for estimating permeability from MICP data are found to have small bias and reasonable precision over a wide range of permeability: the modified Purcell, the Katz-Thompson Lc, Katz-Thompson Lh, and the Swanson methods. A weighted average of these permeability estimates corrects for accuracy problems and increases permeability estimate precision. However, this MICP-predicted average permeability still varies from measured Klinkenberg-corrected steady permeability by an average of a factor of two. This mismatch may be more apparent than real. Restoring reservoir stress prior to conventional permeability measurement fails to remove completely the core damage caused by microfractures created during extraction, preparation, and storage of tight rock samples from deep boreholes. MICP permeabilities are estimated from the pore-throat distributions, which do not include the significant flow contributions from microfractures. Difference between MICP permeability estimates and measured permeability of tight samples may be caused by the inability of conventional permeability analysis to remove damage effects by stress restoration. If so, MICP permeability estimates are as good as or better than permeability measured from tight, subsurface samples. MICP permeability is either the ambient matrix permeability or a stressed matrix permeability, depending on the relative magnitude of in situ reservoir stress and Hg pressure at threshold saturation.

Interpreting Permeability From Mercury Injection Capillary Pressure Data

Alton A. Brown, Consultant, Richardson, TX altonabrown@yahoo.com

Abstract

Laminar flow theory predicts a strong correlation between permeability and pore-throat distribution as revealed by Mercury Injection Capillary Pressure (MICP) data. Previous studies have developed relationships between MICP data and permeability; however, the permeabilities predicted by different methods can differ substantially from the measured permeabilities and from each other, especially in low permeability samples of interest for unconventional reservoirs. The purposes of this study are to evaluate why there is such large scatter, identify algorithms that best predict permeability over a wide range of permeabilities, and evaluate what type of permeability is actually measured by MICP data.

Precision of permeability predictions is ultimately controlled by the size of the MICP pressure steps. MICP permeability estimates of high permeability samples typically lie within the uncertainty controlled by the pressure step size. Four MICP methods estimate permeability in high permeability samples within expected precision and estimate similar permeability for low permeability samples. These are the modified Purcell, the Katz-Thompson L_e, Katz-Thompson L_h, and the Swanson methods.

MICP permeability estimates of low permeability samples have greater than expected scatter and systematically misestimate permeability as a function of measured permeability, even using the best methods available in the literature.

The cause of the systematic estimate difference is the confining pressure. MICP samples are stressed measurements, with confining stress equal to the Hg pressure at threshold conditions. Steady permeability tests are typically measured at one of two pressures, a low "routine" confining pressure and high reservoir pressure. A stress factor that is a function of porosity was developed along with a method to correct MICP permeability estimates to a constant stress. Stress-corrected MICP permeability estimates linearly correlate to measured permeabilities.

The probable cause of high scatter is the nature of the pore system. Pore throat shape does not significantly affect permeability, but more continuous microfractures do. Microfractures contribute to permeability measured in some samples, even at relatively high stress. However, MICP methods estimate matrix permeability only. Where microfractures are artifacts of core recovery and storage, MICP permeability estimates are better than steady permeability measurements.

What Is MICP?

Mercury Injection Capillary Pressure (MICP) is a measure of the volume of mercury (Hg) that can invade pore volume of the rock as a function of the mercury pressure. Mercury does not wet sedimentary rocks surfaces, so the Hg pressure is the capillary pressure. The capillary pressure can be used to calculate effective diameter of pore throats given assumptions about pore-throat shape.

Hg pressures are related to pore-throat diameters by the Young-LaPlace relationship. If Hg surface tension and wettability are known, the cylindrical pore-throat diameter (d) corresponding to a particular Hg pressure (P_c) can be estimated:

$$d = \frac{4T\cos\theta}{P_c} \qquad d\ (\text{microns}) = \frac{213}{\text{Hg psi}}$$

where θ = angle of wettability; T = surface tension; P_c = capillary pressure; d = cylindrical throat diameter. A coefficient of 2 is used where d is the width of an infinite sheet-shaped fracture.

MICP does not measure pore size; it measures accessible pore-throat size. To invade a pore throat, an Hg thread must extend from the sample surface to that throat through pores and throats, all of which must be larger than the invaded pore throat. The MICP curve shows saturation (dependent variable) as a function of Hg pressure (independent variable). The Hg saturation is not the fraction of pore throats; it is the volume fraction of the pore space.

Why Another MICP - Permeability Study?

- Theory predicts strong correlation between MICP parameters and permeability (e.g., Purcell 1949). Permeability measurements of tight samples can be more expensive than MICP tests. Permeability estimation from MICP may be more cost effective than direct permeability measurement if determined to be sufficiently accurate and reliable.
- However, permeability estimated by different MICP methods can differ substantially from the measured permeability and from each other, especially in low permeability samples (e. g., Comisky et al. 2007). The reasons for this mismatch are not clear in the literature.

This study focuses on MICP data quality and methodology of permeability interpretation from MICP data rather than developing new MICP permeability estimation methods or correlations. Critical areas of MICP methodology were identified for improvement, especially by automation of interpreting the MICP parameters needed for permeability estimation. The other problem is a conceptual problem of what type of permeability is estimated by MICP. This is investigated by evaluating the expected effective stress history of MICP samples before and during testing.

General Strategy

- Evaluate data problems before evaluating permeability estimation models. (1) Develop reproducible criteria for identifying conformance and other effects not representing true pore systems. (2) Evaluate effects of MICP pressure table on potential precision of MICP permeability estimation. (3) Correctly extract the incremental saturation curve. (4) Evaluate potential stress effects on sample during data collection.
- Analyze the MICP data directly rather than analyzing model fits such as the Thomeer (1960) or Brooks-Corey (1966) models. The shape of the curve near the threshold pressure has a greater effect on permeability than curve shape at high capillary pressures. By trying to fit the entire curve, the part of the curve critical for permeability may not be fit as well.
- The basic unit for analysis is the pore-throat population as discussed below. A rock may contain several MICP pore-throat populations, each of which is associated with a permeability.
- Work from the incremental MICP curve and the cumulative curve. Incremental curves can be interpreted automatically and thereby avoid possible bias in interpretation methods.

Model Parameters vs. Data Parameters

The Thomeer (1960) and Brooks and Corey (1964) fits require three fitting variables: a threshold pressure (P_t, defined differently for different models), an irreducible water saturation (S_{wi}), and a curvature factor (G in Thomeer and λ in Brooks-Corey). The P_t value is especially critical for permeability estimation. There are no reproducible automatic methods to fit the model P_t or S_{wi} to most MICP data, especially in the presence of significant conformance. Statistical model fits (such as variance minimization) are biased to fit the middle part of the MICP curve where most of the data lie. Because P_t is estimated by the operator, it can be unconsciously chosen to match permeability expectations.

For these reasons, the approach used here considers only permeability models that can be picked from the data instead of parameters from model fits to data.

Why MICP Parameters Correlate with Permeability

Both permeability and Hg pressure are related to the diameter of the pore throat.

Permeability is a tensor commonly represented as a vector in flow models. For flow in any direction, the complex rock pore system can be represented as a system of tubes with variable diameter both along each tube and between tubes (Figure 1). Each increment of the tube has a flow constant (permeability) that is a function of the tube diameter squared and a shape factor (C, Bear 1972): $k = Cd^2$. Narrow pore throats have the greatest flow resistance so they control flow through each tube. Because flow is the sum of the individual tube flows and porosity is the sum of the tube volumes, the most abundant tubes with the largest effective diameters contribute most to the total permeability.

The MICP curve comprises pressure and saturation pairs during injection. The incremental saturation associated with an incremental Hg pressure increase can be interpreted as the volume of tubes with diameter range interpreted from the Hg pressure increment. At pressures where Hg saturation extends across the sample, the tubes contribute to the permeability. Tubes with the lowest Hg pressure (largest throat diameter) and a significant volume (incremental saturation) contributes most to flow.

Relationship. The tube model predicts a squared relationship between permeability and the pore throats in the largest tubes extending across the sample as interpreted from MICP data. The tube model assumption, irregular diameter of model tubes, the contribution to flow by smaller tubes, and the permeability anisotropy of the sample adds scatter to this relationship. However, unless there is a systematic change in tube volume to effective tube diameter as effective tube diameter decreases, the permeability should remain scaled to the inverse tube diameter squared at all permeability ranges.

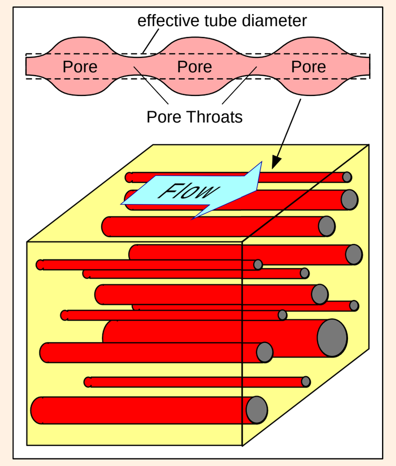

Figure 1. (left) Tube model for permeability. Pores and throats can be represented by tubes with a constant effective diameter (Upper). Effective diameter is close to the throat diameter (e.g. Ehrlich et al. 1991). Permeability in the direction of interest is the sum of the flow in the tubes in that direction (lower).

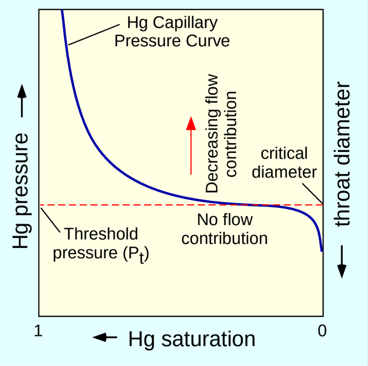

Figure 2 (right). Contribution to permeability by different parts of the MICP curve. Below the threshold pressure, Hg pathways do not extend across the sample, so these large throat diameters do not significantly contribute to permeability. At pressures above the threshold pressure, Hg-saturated throats become smaller and contribute less to permeability. Most permeability is associated with the throat diameter at the threshold pressure (critical diameter) and throats slightly smaller than that diameter.

MICP Permeability Precision

MICP saturation data are collected at pressure steps chosen prior to testing, called the "pressure table". Spacing on the pressure table controls precision (but not accuracy) of any permeability interpreted from that MICP test. Permeability can be no more precise than the increment of permeability between adjacent pressure steps.

A pressure step is converted into a permeability step using the generic inverse-square relationship between capillary pressure and permeability described by laminar flow theory and Young-LaPlace relationship. Because we are converting ratios, other factors cancel out:

$$\frac{k_i}{k_{i+1}} = \left[\frac{P_{i+1}}{P_i}\right]^2$$

The desired permeability precision can be estimated from the number of equally spaced pressure steps between 2 and 60,000 Hg psi (Figure 3, right). Ten percent permeability precision (e.g., 1 vs. 1.1 mD or 50 vs. 55 mD) requires a pressure step ratio near 1.049 and about 200 pressure points between 2 and 60,000 psi. One percent permeability precision (e.g., 1 vs. 1.01 mD) requires about 2000 pressure points between 2 and 60,000 psi. Many industry tests have about 40 points or so, corresponding to a precision of about 40% (e.g., 1 vs. 1.4 mD or 0.71 vs. 1 mD). Poor permeability prediction by MICP is partially due to inadequate number of pressure steps.

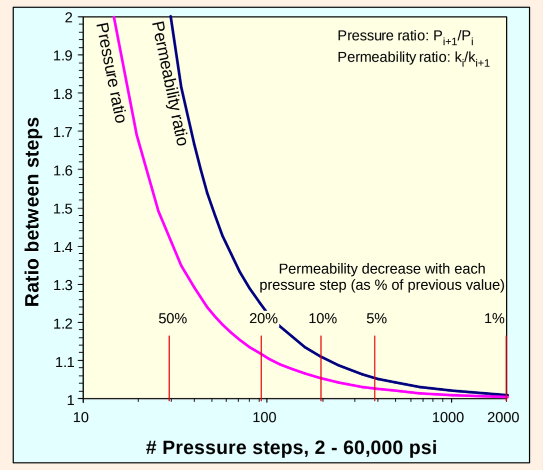

Figure 3. Permeability and pressure ratios associated with the number of logarithmically equal spaced pressure steps between 2 and 60,000 psia. The vertical red lines are the percentage permeability decrease at each increasing pressure step.

Incremental MICP Saturation

Raw incremental data are sometimes interpreted as incremental size distributions. This is not always correct (Lemorand 2003). Many historic MICP data have irregularly spaced pressure steps. Irregular spacing has two effects: permeability precision differs at different pore-throat sizes (Figure 4, right) and incremental saturation curves have to be corrected for irregular spacing.

Larger pressure steps capture more incremental saturation than shorter pressure steps. Incremental curves constructed directly from the reported incremental saturations will be affected by the irregular pressure spacing (Figure 5). The incremental distribution may appear quite irregular and difficult to interpret.

New MICP data should have pressures spaced equally on a logarithmic scale; that is, the ratios between pressure of adjacent steps should be the same for the entire pressure table (Lemorand 2003). To correctly plot incremental curves for historic data with irregular pressure steps, the saturation difference has to be normalized to the pressure differences. In this study, saturation differences are normalized to two different pressure scales, linear and logarithmic (Figure 5).

- Linear normalization. The incremental saturation change is divided by the incremental pressure change. The pressure for the saturation increment is the arithmetic average of the two bounding pressures. The linear-normalized incremental saturation curve is used for flow evaluation (see sheet 2).
- Logarithmic normalization. The saturation difference between steps is divided by the logarithm of the pressure ratio between adjacent pressure steps. This assumes that the saturation is distributed with a logarithmic scale (such as a lognormal distribution) as expected from the central limit theory and Lemorand (2003). The pressure at the saturation increment is the logarithmic average of the bounding pressures. The shape of the logarithmic-normalized incremental curve is close to that of the "as received" incremental curve, but it has a much smoother shape (Figure 5, right). The logarithmic incremental curve peak (mode) is typically smaller than the mode of the linear incremental saturation curve (Figure 5).

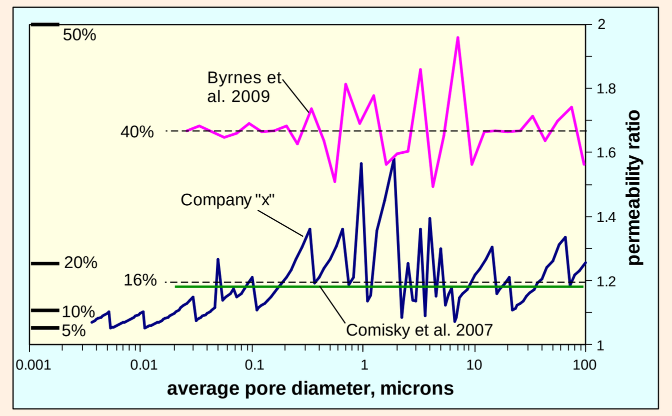

Figure 4. Effect of irregular pressure steps on permeability precision. Colored lines show permeability ratios as a function of average pore diameter at the pressure step. Horizontal lines at left are the percent permeability decrease at each increasing pressure step.

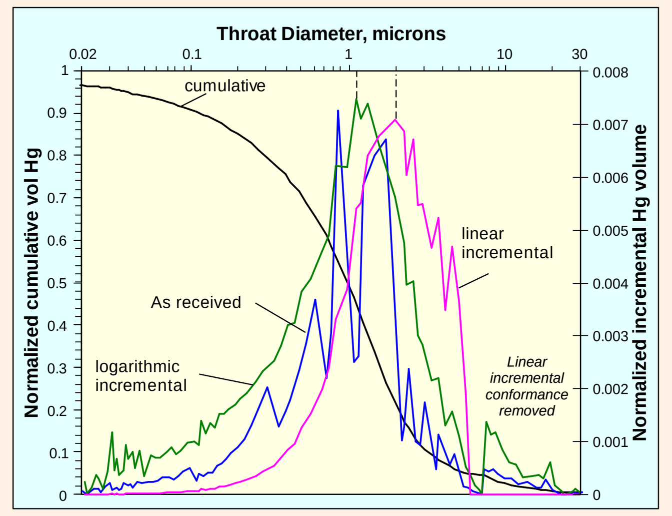

Figure 5. Comparison of cumulative and incremental curves. As received (raw) saturation increment data (blue) are erratic due to unequal pressure steps. Logarithmic incremental data (green) has removed effects of irregular pressure steps. Linear incremental data (pink) is also more systematic, but its peak is at a larger pore throat. Curves are normalized.

Pore Throat Population

The basic unit for permeability interpretation is the pore-throat population. The pore-throat population approach has been previously used (e.g., Clerke 2009), but the throat population is identified differently here, and it is used to interpret up-scaled sample permeability.

A pore-throat population is that part of the total logarithmic incremental saturation curve characterized by a single mode and (typically) a negative skewed normal distribution on a logarithmic throat-diameter scale. Permeability can be calculated for each throat population in the sample.

Where the sample has a single throat population, the sample permeability is that of the throat population and sample permeability is near isotropic. Where a sample has multiple pore-throat populations (figure at right), up-scaled sample permeability is interpreted from the sample fabric and the permeability of each population. With proper fabric interpretation, the matrix permeability vector can be estimated. Contact the author for details.

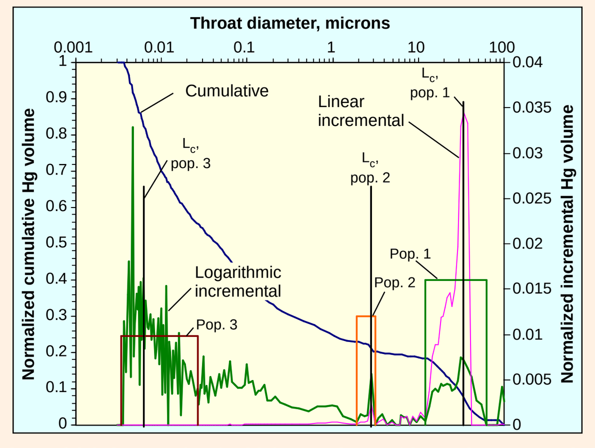

Figure (right) Example of a high porosity muddy sandstone sample with multiple pore-throat populations. Population 3 is broad with a poorly characterized L_c due to sample compaction. Linear incremental curve not shown for coarsest pore-throat sizes.

Conformance and Compaction

The Hg volume reported in the MICP test is a combination of intruded volume, conformance volume, and compaction volume (Figure 6). The easiest way of separating these three effects is inspection of the incremental curves.

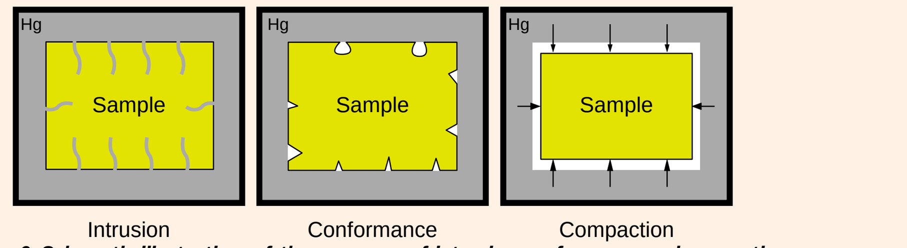

Figure 6. Schematic illustrations of the processes of intrusion, conformance, and compaction.

(1) Intrusion into the natural pore space of the sample. This is the information desired from the MICP test to characterize the pore system. Pore system intrusion is recognized by its systematic lognormal incremental distribution, typically with negative (fine) skewness when plotted against logarithm of throat diameter (Figures 7, 8).

(2) Conformance is Hg intrusion into irregularities on the sample surface and surface damage created by sampling and storage. Conformance is an artifact, so it may not form a lognormal distribution. In sandstones, it is commonly erratic, with greatest variation at lowest Hg pressures (Figure 7). Conformance is especially evident on the linear incremental curve (Figure 8).

(3) Sample compaction. Hg surrounds and conforms to the sample prior to intrusion. Pore space is in vacuum, so the Hg pressure outside of the sample loads the sample. The sample compacts in response to loading by decreasing porosity. Hg volume enters the chamber as the sample compacts, but this volume is pore volume transferred outside the sample by compaction.

Compaction is most evident at Hg pressures below the threshold pressure. Compaction is a smooth function of effective stress. Compaction will therefore form a uniform or slightly sloped incremental saturation curve between the intrusion and conformance (Figure 7, 8). Compaction continues as Hg intrudes into pore spaces, but it is more difficult to identify due to the much larger volume of Hg intrusion. Sample compaction is commonly included with conformance because it is most evident below the threshold pressure.

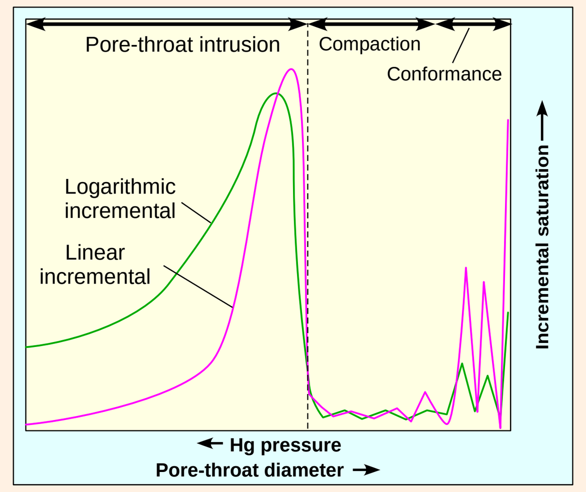

Figure 7. (Idealized incremental curve patterns expected for different causes of increased Hg volume. Conformance causes irregular incremental curves. Compaction forms relatively uniform incremental saturations greater than zero. Pore throat populations have a lognormal distribution with distinct peak (mode) and negative skewness relative to pore diameter.

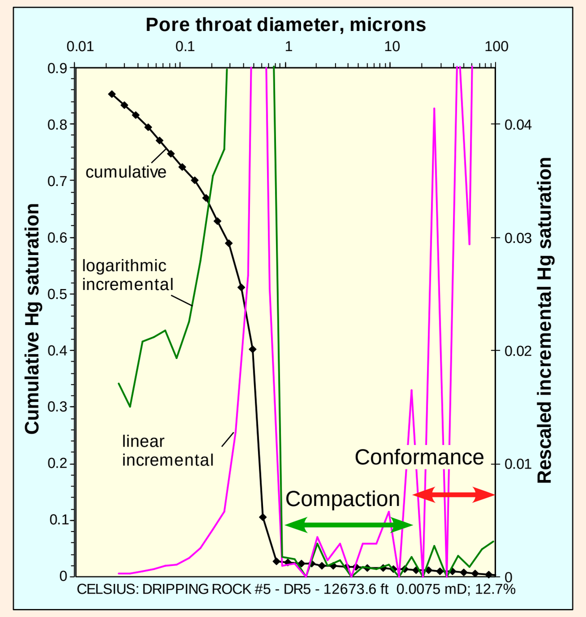

Figure 8. Example incremental and cumulative curve for a sample with conformance (red) and compaction (blue). The logarithmic incremental curve shows a strongly fine-skewed throat population. Incremental curves are scaled up to show variation.

Literature MICP Permeability Methodologies

Four MICP methodologies were found by previous studies to be reliable predictors of permeability in the range of conventional reservoirs: the Purcell (1949) tube flow model as modified by Comisky et al. (2007), The Swanson (1981) air permeability model, and the two Katz and Thompson (1986) models. Other models (Winland in Kolodzie 1980, Thomeer 1983, Walls and Amaefule 1985, Kamath 1992, Pittman 1992, Huet et al. 2005, Dastidar et al. 2007) do not estimate permeability as well in lower permeability samples, are empirical or statistical in nature, or require parameters derived from fitting curves to MICP data. These other models may be valid, but they will not be considered further.

The Katz - Thompson L_e and L_h models (Katz and Thompson 1986, 1987) are the most robust from a theoretical point of view, because they are based entirely on theoretical parameters without empirical fit. The L_e model is based on the throat diameter (critical length, L_c) corresponding to the threshold pressure throat diameter at maximum electrical conductivity (L_e^{max}), and porosity, whereas the L_h model is based on the critical length throat diameter at maximum hydraulic conductivity (L_h^{max}) and porosity. These models are mostly independent, yet both show good to excellent correlation to measured permeability.

K-T L_e model: $$k = \frac{1013}{226} L_c^2 \frac{L_e^{max}}{L_c} \phi S_{L_e max}$$

K-T L_h model: $$k = \frac{1013}{89} (L^h_{max})^2 \frac{L_h^{max}}{L_c} \phi S_{L_h max}$$

L_c is the critical length (the pore diameter at the percolation threshold), ϕ is fractional porosity, L_e^{max} is the throat diameter with the maximum electrical conductivity, and $S_{L_e max}$ is the Hg saturation at L_e^{max}. L_h^{max} is the diameter at maximum hydraulic conductivity, and $S_{L_h max}$ is sample Hg saturation at L_h^{max}. Critical length (L_c) is identified by the change in slope on the Hg saturation vs. Hg pressure curve (Katz and Thompson 1986). This is identical to the maximum of the linear incremental saturation curve. The hydraulic and electrical conductivities are calculated using incremental saturations and diameters calculated from capillary pressure as described in Katz and Thompson (1987).

The Purcell (1949) model is based on the tube flow model. Incremental capillary pressures on the MICP curve are interpreted as effective diameters of tubes, and the incremental saturations are interpreted as the volumes of the tubes. The contribution to flow from tubes of each incremental diameter are summed to give the total permeability (modified from Purcell 1949):

$$k = Cf\phi \sum_{S_{Hg}=100}^{S_{Hg}=0} \frac{S^i_{Hg}}{(P^i_{Hg})^2}$$

Where P_{Hg}^i are average Hg pressure of the increment, S_{Hg}^i are fractional saturations of that increment, C is a constant for converting units (about 14200 for Hg psi, mD, fractional porosity, and saturation in percent), ϕ is fractional porosity, and *f* is an empirical lithology factor. Purcell (1949) used *f* = 0.216; however, Comisky et al. (2007) proposed a value of 0.15 that better fits Klinkenberg-corrected air permeabilities of low permeability rocks. Purcell permeability estimated here will use the value of *f* proposed by Comisky et al. (2007). Purcell's equation is further modified by summing permeability contributions from smallest to largest tubes. This summation direction helps evaluate effects of the upper limit to conductive tube size.

The Swanson (1981) model estimates permeability as a power law of the Swanson parameter:

$$k = aS^b$$

The Swanson parameter (S) is the bulk rock Hg saturation in percent divided by the Hg capillary pressure in psia at the apex of the Thomeer hyperbola. Fortunately, the Swanson parameter can be estimated without determining the Thomeer parameters. The throat diameter at the apex of the Thomeer hyperbola is the diameter at the maximum electrical conductivity, L_e^{max} (Comisky et al. 2007). Alternately, the Thomeer apex occurs at the maximum of the S_{Hg}/P_{Hg} of the data (Pittman 1992; Ma and Morrow 1996). The Comisky et al. approach was used here. The constants proposed by Swanson (1981) for air permeability prediction are a = 389, and b = 1.691 for permeability in mD.

Presented at AAPG ANNUAL MEETING, Denver, 2015

Interpreting Permeability From Mercury Injection Capillary Pressure Data

Test of MICP Permeability Estimation Models

Previous literature studies have provided more comprehensive tests of MICP permeability prediction models than that presented here. See Comisky et al. (2007), Kamath (1992) and Ma and Morrow (1996) for comparisons to different methods. These studies show that no MICP model predicts permeability of low-permeability samples well. Models with strong theoretical basis in the inverse square relationship to capillary pressure (Katz-Thompson models and the Purcell model) should predict low permeabilities as well as high permeability values. The purpose of testing the MICP models here to gain insight into why the models do not better predict permeability in low permeability samples and to use these insights to correct the low permeability MICP estimates to better match steady permeability test measurements.

Data

The data analyzed here is the public domain DOE data (Byrnes, Cluff, and Webb 2009). Samples are archived siliciclastic core material from the Cretaceous-aged Mesaverde formation in various Rocky Mountain basins.

Data include tabulated MICP analyses with porosity and permeability measured on the same samples. MICP measurements extend from 2 to 9,300 psi in 34 pressure steps with permeability precision averaging about 1.6 (Figure 4, sheet 1). Permeabilities are gas permeabilities collected at 600 psi and 4000 psi confining stress. The 4000 psi confining stress permeability data were Klinkenberg corrected whereas the 600 psi permeability data were not. I corrected the 600 psi permeabilities for Klinkenberg effects using the estimated experimental conditions and b factor correlations to permeability developed in the Byrnes et al. (2009) study. Electrical and other properties were collected in the Byrnes et al. (2009) study, but these were measured on samples different from the MICP samples.

Data from other studies have been evaluated, but they not discussed here. These include proprietary data and the summary data presented by Comisky et al. (2007) and Ma and Morrow (1996).

Work flow

Raw He porosity, cumulative and incremental Hg saturations, and Hg pressures were copied into a standardized spreadsheet. The spreadsheet calculates and plots the linear and logarithmic incremental saturations. The conformance and compaction parts of the MICP curve are automatically identified using the incremental curves and fixed parameter cutoffs. The plots were inspected to make sure that maximum real throat size was correctly identified. The logarithmic incremental curve was then used to determine if single or multiple pore-throat populations were present in the sample. This must be done by hand. The number of throat populations is the number of significant modes on the logarithmic incremental curve over the range of throat diameters not affected by conformance and compaction.

Most samples have a single throat population. For these samples, the spreadsheet automatically calculates all parameters needed for permeability interpretation by all tested methods and then calculates the permeabilities automatically (Figure 9). The raw incremental data are used for the Purcell permeability, Swanson parameter estimation, and Katz-Thompson L_e^{max} and L_h^{max} calculation. The linear incremental data are used to estimate L_c (K-T threshold diameter). Because no parameter used for permeability estimation is arbitrarily selected by the operator, there is no potential for inadvertent bias to permeability estimates.

Samples with multiple throat populations were analyzed slightly differently. The pore diameter forming the boundary between the throat populations was picked by hand at the minimum logarithmic incremental saturation between the modes for the two populations. The permeabilities for each of the throat populations are calculated automatically in a manner similar to that of the single mode samples, only over the range of pore throats specified within each population and with porosity for each population based on the saturation at the division between the two populations. The throat population with the highest permeability was used for testing. There are few multiple throat populations in the DOE data, so the arbitrary selection of the most permeable throat population does not greatly affect overall results.

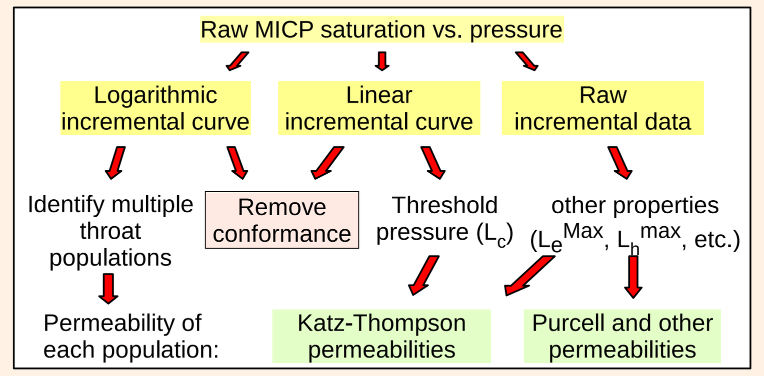

Figure 9. Schematic work flow for interpreting permeability from MICP data in DOE database. The logarithmic incremental curve was used only to remove conformance and identify the number of throat populations. The linear incremental curve was used both to remove conformance and to interpret K-T threshold pressure. Raw incremental data were used for other K-T parameters, Purcell permeability, and Swanson number.

Results

Permeability predicted by the 4 examined methods cluster within about a factor of 3 of each other at permeabilities greater than 1 microDarcy. At lower permeability, scatter between estimates increases (Figure 10).

Part of the scatter is systematic with type. K-T L_h estimates are about 40% higher than K-T L_e estimates at permeabilities greater than a microDarcy and converge at lower permeabilities. Swanson air permeability estimates also average above 40% higher than the K-T L_e estimates, but scatter is much greater. Swanson permeability scatter increases below 1 microDarcy. Modified Purcell permeability is similar to the K-T L_e permeability above about 1 microDarcy and underestimates it by about a factor of 2 or so at lower permeability.

The between-method scatter may be partially related to the broad spacing of pressures because permeability differences fall within the precision limit related to pressure step size. However, even tests with small pressure differences will have different permeability estimates by different MICP methods. It is possible to take advantage of this scatter to increase precision of the MICP estimate. Average the different reliable MICP permeability estimates, and, if differences are statistical and unbiased in nature, the average is likely to converge on the real permeability. If there are systematic differences between methods, these can be corrected before averaging. Based on Figure 10, average MICP permeability for this study can be defined as:

$$k_{avg} = (1.2k_{Le} + 0.9k_{Lh} + 0.9k_s + 1.1k_{mp})/4.$$

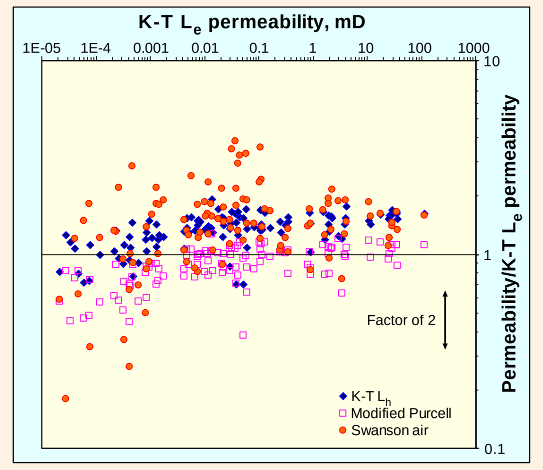

Figure 10. Comparison of different MICP permeability estimates. Horizontal axis is K-T L_e permeability estimate. Vertical axis is the ratio of other MICP permeability estimates to the K-T L_e estimate. Factor of 2 difference is indicated by the vertical arrow.

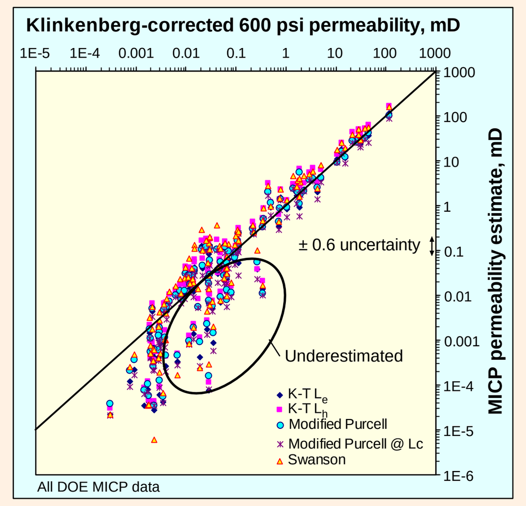

Figure 11. Comparison of MICP estimated permeability to 600 psi Klinkenberg-corrected measured permeability for DOE samples (Byrnes et al. 2009). In general, MICP methods estimate measured permeability within expected uncertainty at high measured permeability. MICP overestimates the permeability of most lower permeability samples, but there is a large subset of samples where MICP methods underestimate measured permeability (circled). MICP methods underestimate permeability of most samples tighter than about 0.005 mD.

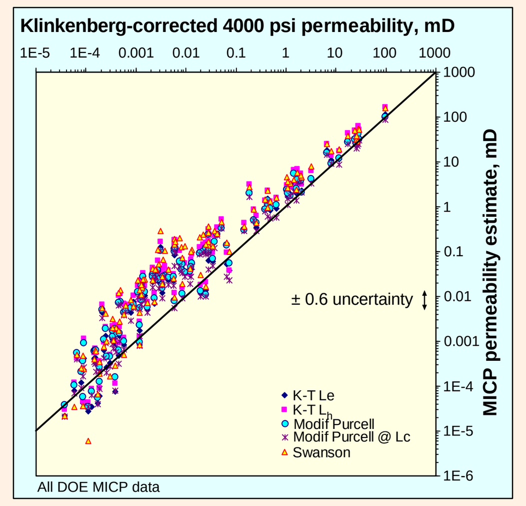

Figure 12. Comparison of predicted permeability to 4000 psi Klinkenberg-corrected permeability for DOE samples (Byrnes et al. 2009). MICP methods overestimate permeability in almost all samples with permeability exceeding 0.0005 mD. Deviation of estimated and measured permeability follows the same general shape as with the 600 psi data, only MICP methods overestimate 4000 psi permeability measurements even more than the 600 psi measurements. Trend scatter is significantly reduced.

Comparison to DOE 600 psi Permeability (Figure 11)

Estimated permeability of samples with permeability above about 0.1 mD lie within the uncertainty range expected for the MICP pressure steps. This indicates that fit is about as good as could be expected.

Samples with permeability less than about 0.1 mD have much poorer correlation between estimated and measured permeability. Most MICP permeability estimates are slightly higher than 600 psi permeability between 0.1 and 0.005 mD 600 psi permeability. However, there is a significant subset of samples where MICP permeability estimates are much lower than the measured 600 psi permeability (circled). This significantly increases scatter in this permeability range. MICP methods significantly underestimate the 600 psi permeability of all samples with 600 psi permeability below 0.005 mD.

Comparison to DOE 4000 psi Permeability (Figure 12)

Permeability estimates for the DOE samples do not change; the different trend is caused by differences between 600 psi and 4000 psi stressed permeability measurements. All samples have 4000 psi stressed permeability less than the 600 psi stressed permeability (Byrnes et al. 2009).

MICP methods systematically overestimate 4000 psi stressed permeability in high permeability (>0.1 mD) samples. MICP methods greatly overestimate measured 4000 psi confined stress permeability of samples with permeability between 0.1 mD and 0.0001 mD. The samples where MICP methods underestimate 600 psi permeability are not underestimated in the 4000 psi data. This results in less scatter to the overall trend. The MICP estimates converge with measured 4000 psi permeabilities at about 0.0001 mD measured permeability. The overall trend of estimated to measured 4000 psi permeability is similar in general shape to that of the 600 psi permeabilities, but shifted higher.

Summary Observations, DOE Data Test

- MICP permeability estimates by the four methods are similar to each other (within about a factor of 3). Modified Purcell permeability estimates of samples with less than 1 microDarcy are a bit lower than other estimates and Swanson estimates show greater scatter.
- MICP permeability estimates are similar to the 600 psi stressed permeability measurements for samples with greater than 0.1 mD. Scatter is approximately within the range expected from the pressure step magnitude.
- MICP permeability estimates for samples with measured permeability between about 0.1 mD and 0.1 microDarcy are not similar to either the 600 or 4000 psi stressed measured permeability. Most measured permeabilities are overestimated by MICP methods.
- A significant subset of samples have MICP permeabilities that significantly underestimate 600 psi permeabilities yet overestimate 4000 psi permeabilities. This may be related to fractures unclosed at 600 psi confining stress.
- The MICP permeability estimates have the same general trend shape to both 600 and 4000 psi permeabilities. Offset between MICP estimates and measurements is greater for the 4000 psi data, yet their scatter is less.

Permeability and Stress

Mismatch between MICP permeability estimates and measured permeability is clearly affected by the magnitude of the permeability and the confining stress applied to the sample during permeability measurement. It is proposed that the difference between MICP test confining stress and permeability measurement confining stress is the main cause of the systematic difference between MICP and measured permeability estimates in low permeability samples.

Stress State During MICP Measurement

Prior to Hg intrusion, mercury surrounds the sample, and the sample is hydrostatically stressed at a pressure that is equal to the Hg pressure. Pore pressure is zero (vacuum). Sample effective stress is therefore the Hg pressure. After Hg intrudes into the pore system, the Hg pressure in invaded pores equals the Hg pressure surrounding the sample. Effective stress is therefore zero in invaded pore throats.

At Hg pressure just below the threshold pressure, the conductive pore throats are not yet invaded and Hg saturation is low (Figure 13). The effective stress associated with the threshold diameter measurement is approximately the Hg pressure. The effective stress associated with a particular MICP permeability estimate is therefore approximately the Hg pressure needed to invade the pore throat that is the main control on permeability.

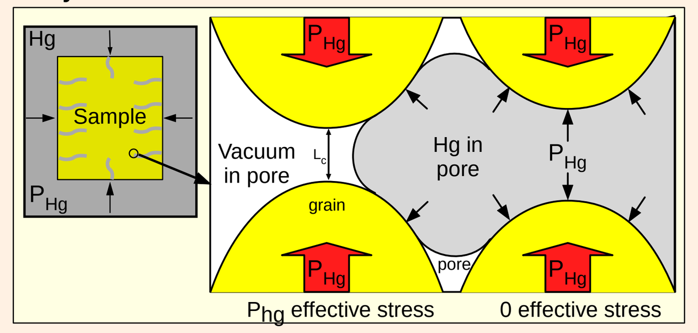

Figure 13. Cartoon of pressure distribution just below Hg pressure needed to invade pore throats at the critical diameter. Left: macroscopic view showing Hg surrounding sample providing confining pressure equal to P_{Hg}. Right: On the microscopic scale, the pore pressure depends on Hg intrusion. At the critical throat, pore pressure is zero just below intrusion pressure, and the effective stress is the Hg pressure. Invaded throats (right) have pore pressure equal to Hg pressure surrounding the sample, so their effective stress is zero.

The magnitudes of effective stresses corresponding to different permeability samples will be illustrated using the Katz-Thompson L_e permeability (Katz and Thompson 1986).

The main control on Katz-Thompson L_e permeability is L_c, the critical diameter at threshold conditions. A secondary effect is the electrical conductivity ratio, which is controlled by L_e^{max} , Hg saturation at L_e^{max} , and porosity (Katz and Thompson 1987). The DOE data were used to determine typical values for these variables so that a generic permeability can be estimated from L_c alone. Porosity correlates to L_c (Figure 14). L_e^{max} correlates to L_c and is typically 0.57 times L_c (Figure 15). Hg saturation at L_e^{max} is variable, but averages about 40% (Figure 16).

Figure 17 shows the K-T L_e permeability plotted against the Hg pressure (effective stress) at threshold conditions. As permeability decreases, Hg pressure at threshold conditions increases. L_e permeabilities near 0.01 mD have the 600 psi confining stress used for DOE routine permeability tests. L_e permeabilities near 0.0001 mD have the 4000 psi confining stress used for stressed DOE permeability measurements.

The Katz-Thompson L_e and L_h permeabilities measure permeabilities at similar confining stresses because both methods depend on L_c. Swanson permeability is a measure of permeability at higher confining stress because Hg pressure at the apex of the Thomeer hyperbola is always higher than that at L_c. However, the sample is partially saturated at the apex and stress state at uninvaded apex pore throats is more ambiguous. The Purcell method uses multiple pore throats, but permeability is controlled most by the largest diameter throats in the throat population, which is similar to L_c. Overall, the relationship of MICP permeability estimate to confining stress at that permeability is similar for all methods.

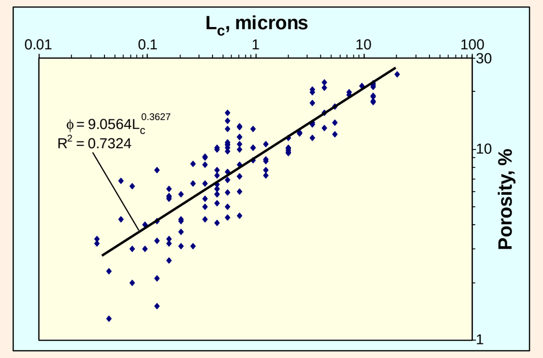

Figure 14. Routine porosity as a function of the Katz-Thompson critical length, L_c. Regression equation (black line) was used to estimate porosity for relationship between K-T L_e permeability and Hg pressure. Data are samples with MICP analyses in the DOE study (Byrnes et al. 2009).

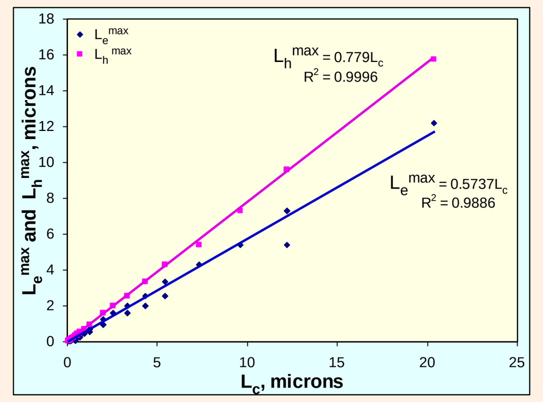

Figure 15. Throat diameters with maximum electrical (L_e^{max}) and hydraulic (L_h^{max}) conductivity as a function of L_c. All parameters calculated using the approach of Katz and Thompson (1987) using MICP sample data from the DOE database (Byrnes et al. 2009). Precision of L_e^{max} and L_h^{max} are limited by pressure step spacing.

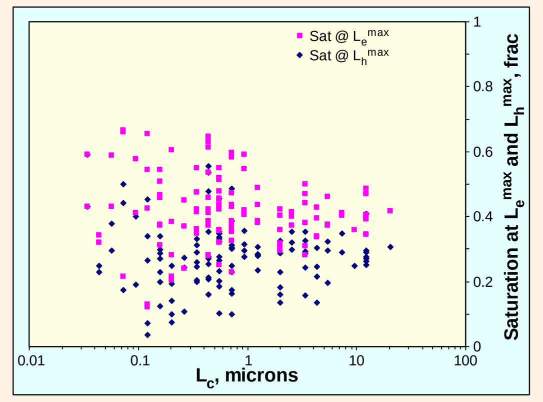

Figure 16. Hg saturation at the diameter with maximum electrical (L_e^{max}) and hydraulic (L_h^{max}) conductivity as a function of L_c. All parameters calculated using the approach of Katz and Thompson (1987) using MICP sample data from the DOE database (Byrnes et al. 2009).

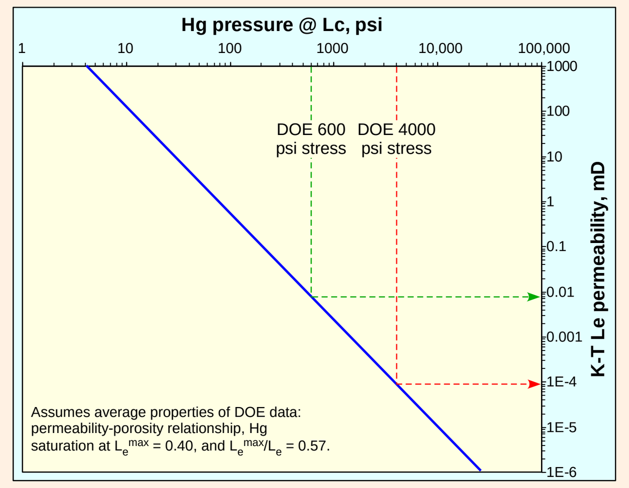

Figure 17. Hg pressure at L_c plotted against the Katz-Thompson L_e permeability. Because these are threshold conditions, Hg pressure is also the effective stress at which the permeability was estimated. As permeability decreases, the Hg threshold pressure and effective stress at threshold conditions increase. K-T L_e permeabilities associated with effective stresses equal to the 600 and 4000 psi confining stress used in the DOE study (Byrnes et al. 2009) are indicated by the thin dashed lines. Other parameters controlling L_e permeability are correlated to L_c as shown by figures below.

Model for Stress Effects on MICP Permeability

Systematic mismatch between MICP permeability estimates and steady permeability measured in low permeability samples is interpreted to be mainly an effect of different confining stresses during MICP measurement and the steady permeability measurements.

DOE permeability measurements were made at two confining stresses (4000 and 600 psi). Confining stress of MICP permeability estimates are a function of the permeability of the sample. The effects of stress on measured permeability will be quantified below, and the stress-permeability model will be applied to the MICP data to convert the estimated MICP permeability to a permeability at constant confining stress.

Confining Stress Affects Permeability

Many studies have demonstrated that confining stress significantly reduces permeability of dry tight sandstones (e.g., Thomas and Ward 1972, Jones and Owens 1980, Walls et al. 1982, Bower and Morrow 1983). The permeability decrease with increasing stress at low confining stress is different in different rocks. The relationship approximately follows a power-law relationship at higher confining stresses, based on both data (Thomas and Ward 1972) and the relationship of Bower and Morrow (1983) if a broad population of throat aspect ratios is assumed.

A permeability stress coefficient was calculated for the DOE study samples based on assumed power law relationship at high confining stress. The stress coefficient (S) is the exponent of power-law relationship between the two confining stresses used (600 psi and 4000 psi):

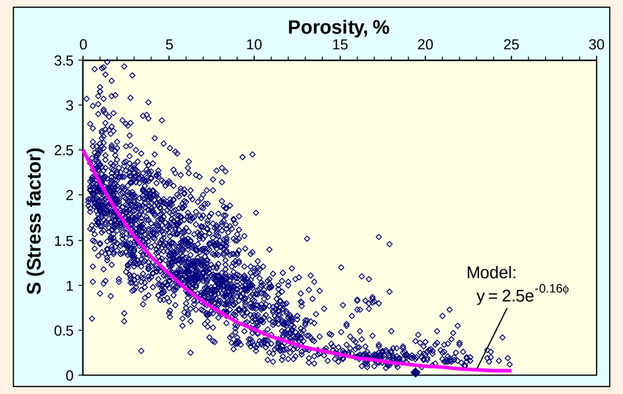

Figure 18. Stress coefficient for permeability calculated from 4000 and 600 psi confining stress permeability plotted against porosity for all DOE samples. Stress sensitivity increases (larger S) as porosity decreases. Discussed model is shown by pink line. Modeled S is less than one over range of potentially economic tight-gas reservoir porosities (8%+).

$$S = -\log(K_{4000}/k_{600})/\log(4000/600) = -\log(k_{4000}/k_{600})/0.8239.$$

S increases as porosity decreases (Figure 18). S data were correlated to percent porosity using an exponential model:

$$S = 2.5\exp(-0.16\phi) \text{ (porosity in percent)}$$

The model is fit to the lower part of the data cloud rather than a least-squares fit (Figure 18). Regression fit was not used because many 600 psi samples show evidence for fracture contribution to flow that give anomalously high S values. A regression fit containing these data will overestimate S for unfractured tight samples.

Adjusting MICP Permeability to Constant Stress

The effective stress of the MICP permeability estimate increases as the MICP permeability decreases (Figure 17). We can adjust the MICP permeability to a permeability at the confining stress of the steady flow tests using the S values:

$$k_r = k_i*(P_i/P_r)^S$$

where k_r is permeability at reference confining pressure P_r, k_i is estimated MICP permeability at P_i Hg pressure, and S is the stress coefficient calculated from the sample porosity (Figure 18). This relationship assumes only the power-law stress sensitivity for permeability.

To understand the general nature of the MICP permeability stress correction, the generic L_e permeability vs. Hg pressure trend of Figure 17 will be combined with the general relationship between S and porosity (related to L_c using Figure 14). Because other MICP permeability estimation methods give estimates similar to the L_e permeability (Figure 10), the pressure correction trends will be similar for all MICP techniques.

At high permeability, MICP L_e permeabilities corrected to 4000 psi and 600 psi confining stress are both slightly less than uncorrected permeability (above 1:1 line on Figure 19). As permeability decreases, the trends diverge from the 1:1 line even further until they reach a maximum divergence from the 1:1 tend. The trends then steepen. At permeability ~0.01 mD for 600 psi and ~0.0001 mD for 4000 psi, the pressure-corrected permeability equals uncorrected permeability. Pressure-corrected permeabilities below these values exceeds uncorrected permeability (trend below 1:1 line). The trends become almost vertical near 10 nD L_e permeability.

The general pattern of MICP permeability deviation from 1:1 trend is the same as that seen between permeability measured at constant stress and MICP permeability (Figures 11, 12). This supports the contention that the major cause for divergence between MICP permeability estimates and measured permeability is the confining stress during MICP test. The systematic difference is not an error in flow theory underlying the MICP permeability estimation methodology.

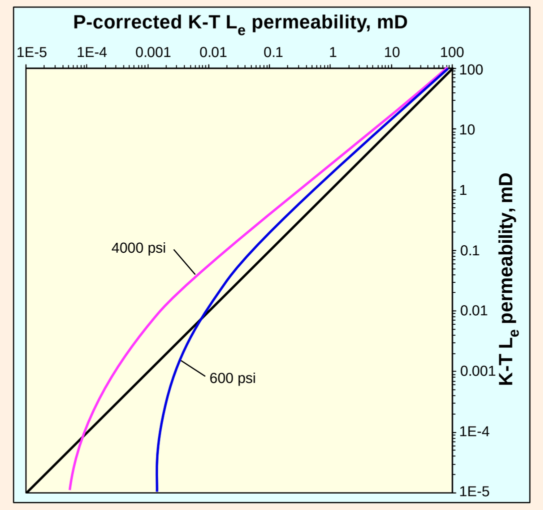

Figure 19. Trend of Le permeabilities corrected to 4000 psi (Pink) and 600 psi (Blue) confining stress (horizontal axis) against MICP-derived L_e permeability (vertical axis). Pressure-corrected permeabilities are estimates of the steady permeability based on S values and MICP permeabilities. Compare trends to those of Figures 11 and 12.

Presented at AAPG ANNUAL MEETING, Denver, 2015

Interpreting Permeability From Mercury Injection Capillary Pressure Data

Stress-Corrected MICP Permeabilities

Values of S and L_c were calculated for all MICP data. These data can be used to correct the individual L_e permeability to desired stresses without using the generalized S vs. porosity trend. L_e permeability corrected to 600 and 4000 psi confining stress are compared to the measured steady permeability at 600 and 4000 psi in Figures 20 and 21, respectively.

Trends between measured and pressure-corrected permeability are linear on log-log plots with slope close to 1 (i.e., a nearly linear relationship; Figures 20, 21). The pressure correction has removed the systematic trend variations seen on the uncorrected MICP permeability plots (Figures 11 and 12). Many corrected MICP L_e permeability estimates now lie within the expected ± 0.6 uncertainty from measured permeability over the entire measurement range.

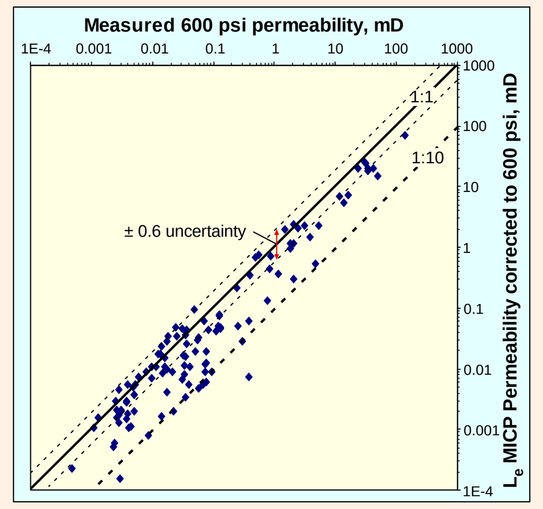

Figure 20. Comparison between MICP L_e permeability estimates adjusted to 600 psi (vertical axis) and measured steady permeability at 600 psi confining stress (horizontal axis).

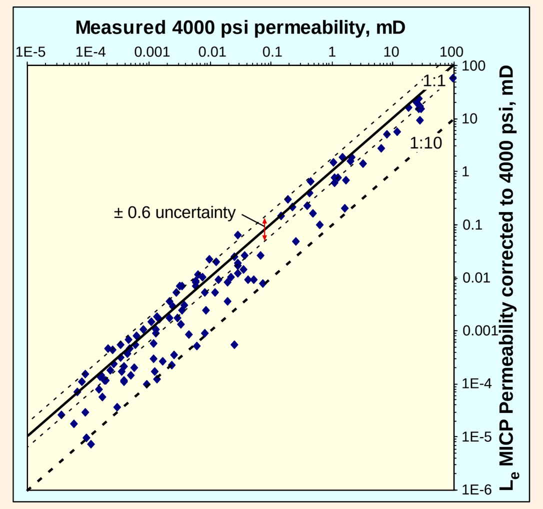

Figure 21. Comparison between MICP L_e permeability estimates adjusted to 4000 psi (vertical axis) and measured steady permeability at 4000 psi confining stress (horizontal axis).

Stress History of Samples

Figure 22. Stress and strain history of subsurface samples. See text for discussion.

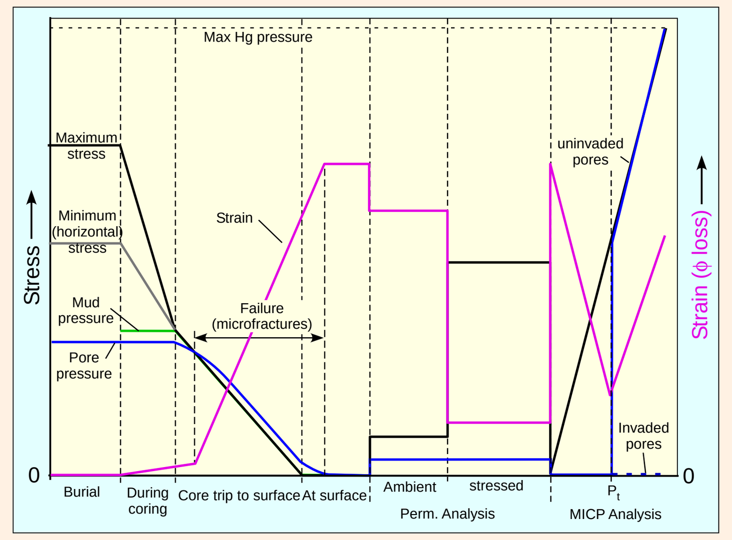

Tight subsurface samples analyzed for permeability are likely to be damaged (fractured) due to variation of the stresses applied to the sample during core recovery and storage. During coring, rock becomes hydrostatically stressed at the mud pressure (Figure 22). As core is tripped to the surface, mud pressure decreases. In permeable core, mud and pore pressure equilibrate during core recovery so overpressure does not develop in the core. In tight rocks, confining (mud) pressure may decrease faster than pore pressure as core is rapidly tripped to the surface. The high pore pressures dilates the sample (forms microfractures). Damage continues during storage until residual pore pressure bleeds off. Force of crystallization from residual salt precipitation and mineral oxidation may also form fractures.

Core samples plugged for permeability analysis are probably damaged if tight. Confining stress during routine analysis heals some damage, but confining stress during routine permeability measurement is too low to close most microfractures in tight samples, so routine analysis is likely to be overestimate reservoir permeability (Jones and Owens 1980). "In situ" or reservoir stressed permeability uses an hydrostatic stress equal to the maximum effective stress at reservoir conditions (Figure 22). However, restored stress is hydrostatic rather than the original anisotropic stress. Restoring stress condition may not restore the permeability of tight samples to its value prior to coring (Byrnes et al. 2009).

There is almost no way to tell if permeability has been properly restored, even at reservoir confining stress. Deviations between MICP permeability estimates and measured permeability could reflect the poor quality of permeability restoration during the test rather than poor quality of MICP permeability estimates.

Possible Causes for Scatter

Stress correction does not remove the scatter between stress-corrected MICP permeability estimates and measured permeability shown on figures 20 and 21. Although many samples fall within the ± 0.6 uncertainty window, many stress-corrected MICP permeabilities underestimate measured permeability. Measured permeability of some samples is underestimated by up to a factor of about 10. Some samples have overestimated permeability, but those samples lie within the uncertainty window. Stress-corrected permeability of the higher permeability samples are almost all underestimated by an average 30 - 40%.

There are several possible causes to the large scatter to the stress-corrected permeability:

1. Incorrect values of S. S data show significant scatter (Figure 18). Incorrect stress adjustment undoubtedly contributes to the scatter, but it is probably not responsible for the high overall scatter. First, scatter estimated from sample S values is similar to scatter estimated from S calculated from the porosity correlation (not figured here). Second, the range of scatter in the uncorrected L_e permeability at any measured permeability (Figure 12) is similar to that of the pressure-corrected L_e permeability (Figure 21).

2. Dual porosity system (Matrix + fracture permeability). Fractures may occur either as sheet pore throats in the matrix system or as a separate fracture pore system (Figure 23). Fractures as a separate pore system may significantly enhance permeability with little porosity increase.

The steady permeability test measures transmissibility through the matrix pore system and any open fractures. MICP methods only estimates flow through throats of the matrix pore system, because a fracture pore system will have too low of a pore volume to form a throat distribution on the incremental curve. MICP permeability estimates are therefore better measures of matrix permeability than steady flow measurements.

If fractures are responsible for the permeability difference shown in figures 20 and 21, it is possible to characterize the fracture system necessary to cause the additional permeability. Fracture widths were assumed equal to L_c and 2.5 times greater than L_c. Fracture permeability was assumed to be nine times greater than matrix permeability for any L_c value. The calculated parameter is the fracture frequency needed to reach this permeability (Figure 24).

Fracture frequency of 5 to 40 fractures/cm explains total permeability assuming fracture width 2.5 times L_c. This frequency is reasonable for typical plug samples. Much higher fracture frequency is needed (40 - 500 fractures/cm) to match permeability where fracture width equals L_c. Fracture frequency for fractures this narrow is probably unreasonably high for intact plug samples. This indicates that a fracture system, if present in the plug, has effective apertures much larger than L_c.

3. Variation in pore-throat shape. Flow models used in MICP permeability interpretations assume cylindrical pore throats. A pore system with percolation behavior can have throats that are sheet shaped instead of the assumed tube shape (Figure 23). The transmissibility change between pores caused by the throat shape factor will change total permeability of the pore system. Variation in pore throat shape can cause permeability variations that may account for the scatter in Figures 20 and 21.

The ratio of the permeability of a single sheet pore throat of width w to a tube pore throat of diameter d is $k_s/k_t = 32w^2/12\alpha d^2$, where α is the length/width of the sheet throat. At equal capillary pressure, sheet throat width (w) is half the tube throat diameter (d) and $k_s/k_t = 2/(3\alpha)$.

The Purcell tube model approach assigns tube size from capillary pressure and tube number estimated from incremental porosity. At each capillary pressure step, the ratio of sheet to tube flow permeability is $k_s/k_t = 2\pi(T_t/T_s)/3$, where T is tortuosity. The aspect ratio cancels out, and the permeability ratio is approximately twice the tube to sheet tortuosity ratio.

Total electrical tortuosity of the DOE data show a scatter that increases with decreasing permeability. In tight sandstones with similar permeability, tortuosity varies by up to a factor of 3 (Figure 25). Removing the Kozeny-Carmen porosity contribution and geometric factor from T gives the path length tortuosity, t^2 (Clennell 1997). Electrical path length tortuosity varies by up to about a factor of 4 and no longer correlates to porosity or permeability (Figure 25). These magnitude variations are insufficient to explain the total scatter of stress-corrected permeability estimated from MICP.

The Katz and Thompson (1986) L_e permeability can also be modified for sheet-shaped pores to evaluate the magnitude of the permeability change. The critical length (L_c) of a sheet pore throat is half that of a tube at the same Hg pressure. The throat geometric factor also changes from 32 (tube) to 12α (sheet). The sheet K-T L_e permeability becomes $1013/(333\alpha) l_c^2 \sigma/\sigma_o$ where σ/σ_o is 1/electrical formation factor (F). F varies by up to about a factor of 10 in low permeability samples with similar permeability (Figure 26). This degree of formation factor variation is sufficient to explain the predicted to observed permeability differences.

The value of α can be estimated by dividing the stress-corrected sheet L_e permeability using α = 1 by measured permeability and a generalized F vs. permeability relationship (Figure 26). Pore throat α calculated from the sheet K-T L_e permeability and measured permeabilities is between 0.1 and 1 (Figure 27). Sheet-shaped pore throats with alpha > 0.1 are not very stress sensitive (Bower and Morrow 1983, Bowers and Katsube 2002). The high compressibility of some tight sandstones may be related to the separate fracture system compressibility.

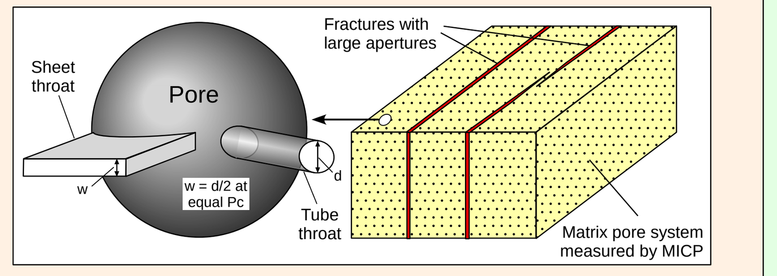

Figure 23. Microfracture concepts. Left: "Microfracture" pore throats. In a matrix pore network, pore throats may be sheet (left) or tube (right) shaped. Sheet pore throat systems should be similar to tube throat systems except for flow properties of the throats. Right: Dual pore system. Sparse, relatively large fractures cross the matrix pore system and do not form a percolation network on the sample scale. The matrix pore system is described by the MICP lognormal incremental pore-throat distribution. Large fractures are not identifiable on the MICP curve due to their small volume.

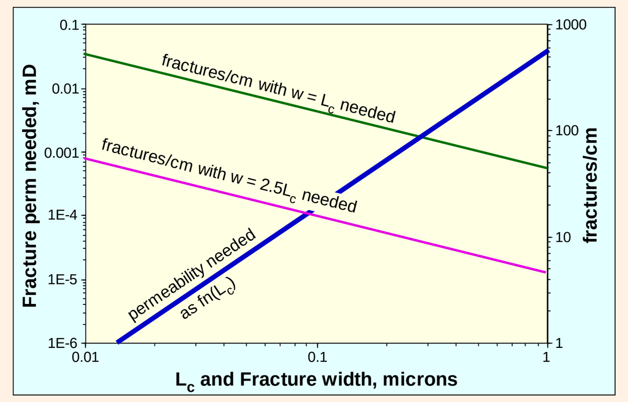

Figure 24. Permeability contribution from fractures needed in dual porosity system to increase total permeability by factor of 10 using fractures with assumed width equal to L_c and 2.5 times L_c. Fracture permeability is increased by increasing the fracture frequency in the sample.

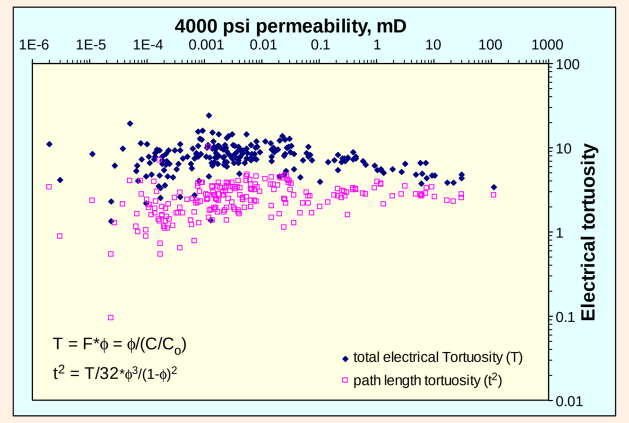

Figure 25. Electrical tortuosity calculated for DOE data. Increasing total tortuosity with decreasing permeability is a porosity effect that is removed by calculating the path length tortuosity (t).

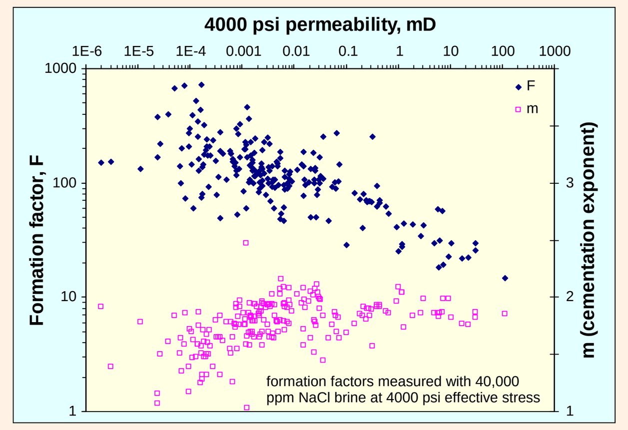

Figure 26. Formation factor (F, blue diamonds) and cementation exponent (m, pink squares) as a function of 4000 psi permeability. F and m were measured with 40,000 ppm NaCl brine at 4000 psi confining stress. Samples are different from those used for MICP measurements. Data from Byrnes et al. 2009).

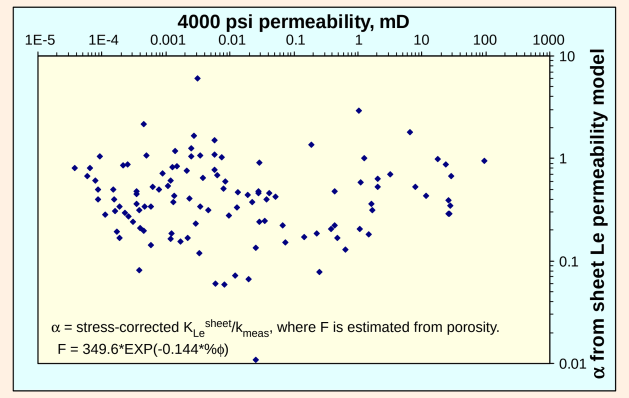

Figure 27. Fracture width/length (α) as function of 4000 psi permeability. Calculated values of α are lower than expected for stress-sensitive rocks. The α values are calculated from data in Byrnes et al. (2009)

Microfractures: Reservoir or Induced?

MICP permeability estimates differ from steady permeability measurements due to two effects: (1) different (and variable) confining stress and (2) different pore system analyzed. MICP estimates permeability of the matrix pore system, whereas steady flow experiments measure the total pore system which may include microfractures. Some measured permeabilities show evidence for fracture contribution to flow, even at 4000 psi confining pressure. These samples have low cementation exponents (m, Figure 26) and stress-corrected MICP permeability significantly less than measured permeability (Figure 21).

Matrix permeability of tight sandstone is estimated by calculating MICP permeability as discussed and correcting the permeability to the stress conditions of interest using the porosity-stress factor correlation. Permeability estimated by this approach is matrix permeability which is the minimum sample permeability at reservoir conditions (fractures only add to the permeability). Total permeability at high confining stress (matrix plus microfracture permeability) probably lies between the matrix permeability and a value ten times higher than matrix permeability, based on Figures 20 and 21.

The presence of microfractures at reservoir conditions is a critical issue for evaluating reservoir permeability. It is easy to form microfractures during recovery of tight cores (see panel below left and Figure 22). Presence of fractures in core samples is not definite evidence for fractures at reservoir conditions. Perhaps the best way for determining fracture contribution to flow is by comparison of production test permeabilities to permeabilities estimated from MICP.

Figure 28. Schematic pore and pore throat geometries in tight sandstones. Pores may be equant (left) or sheet shaped (right). Sheet pore throats may occur with either pore type. Because most porosity is in pores rather than pore throats, low porosity sandstones are more likely to have sheet-shaped pores and sheet-shaped throats. Pores are much too large to limit flow, because critical lengths of tight rocks are less than a tenth micron. Permeability sensitivity comes from aspect ratios of the pore throats, not the pores. A sheet throat that is a tenth micron wide and 40 microns long has an aspect ratio of 400 which is sufficiently high to cause observed permeability stress sensitivity. Most petrographic studies report pore aspect ratios and not throat aspect ratios.

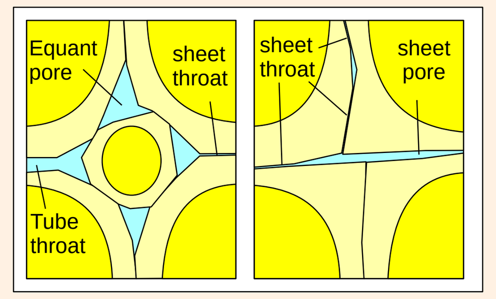

Summary and Conclusions

The main reasons that MICP permeability estimates do not match measured permeability of tight sandstones are the following (in decreasing order):

(1) MICP permeability estimates are measured under a confining stress approximately equal to the Hg threshold pressure. Tight sandstone permeability is strongly pressure sensitive. Different confining stress causes a non-linear trend of logarithm of MICP permeability against logarithm of measured permeability. MICP permeability estimates have to be adjusted to the stress of the steady permeability test for comparison to measured permeability. A simple stress coefficient of permeability (S) is introduced for correcting MICP permeability estimates using measured sample porosity.

(2) MICP permeability methods measure matrix permeability only and do not measure the permeability contribution from fractures forming a second pore system in the sample. Permeability measured by steady flow tests of samples with fractures will be greater than the stress-corrected MICP permeability estimates. MICP methods may estimate reservoir permeability better than steady permeability tests where reservoirs do not have in situ microfractures.

(3) MICP permeability has precision limited by the ratio of pressure steps. High precision MICP permeability estimation is operationally difficult due to the large number of pressure steps required to achieve adequate permeability precision. Precision can be somewhat improved by averaging MICP permeability estimates by the four reliable MICP methodologies.

(4) Precision and accuracy of MICP permeability in prior studies is also limited by hand picking the parameters used for permeability estimation. Hand picking parameters can introduce bias into calibration and test data sets. Methods for automatically picking MICP parameters were developed as part of this study. Autopicking removes this potential operator bias.

Recommended General Work Flow for MICP Permeability Estimation

(A) For new data, choose as homogeneous of sample as possible for analysis to avoid anisotropy and heterogeneity effects. Use equal logarithmic pressure steps. Select the number of pressure steps that are suitable for desired permeability resolution.

(B) Enter MICP data into a spreadsheet, calculate incremental pore-throat distributions, and have the spreadsheet automatically pick MICP parameters using arbitrary, consistent criteria for estimating these parameters. This avoids bias that may result from hand picking parameters.

(C) Interpret MICP permeabilities by the different reliable methods (K-T L_e, K-T L_h, Swanson, modified Purcell). Average these reliable MICP permeability estimates to improve precision. Use multipliers to remove any small amounts of bias by the different methods where judged necessary.

(D) Correct MICP to confining stress of interest using sample porosity and the empirical stress-correction factor (S) equation or similar relationship developed for lithologies of interest.

References

Bear, J., 1972, Dynamics of fluids in porous media: (1988 reprint by Dover Publications, New York) 764 p.

Bower, K. R. and N. R. Morrow, 1983, Fluid flow in cracks as related to low permeability gas sands: 1983 SPE/DOE Symposium on low permeability, Denver CO, March 14-16, 1983, p. 201 – 212; SPE/DOE 11623.

Bowers, G. L., and T. J. Katsube, 2002, Chapter 5: The Role of Shale Pore Structure on the Sensitivity of Wire-Line Logs to Overpressure: *in*: Pressure Regimes in Sedimentary Basins and Their Prediction (A. Huffman and G. Bowers, eds.), AAPG Memoir 76, p. 43-60.

Brooks, R. H. and A. T. Corey, 1964, Hydraulic Properties of Porous Media: Hydrology Paper No.3, Colorado State University, Fort Collins, Colorado.

Byrnes, A. P., R. M. Cluff, and J. C. Webb, 2009, Analysis of Critical Permeability, Capillary Pressure and Electrical Properties for Mesaverde Tight Gas Sandstones from Western U.S. Basins: US DOE # DE-FC26-05NT42660 Final Scientific/Technical Report: pdf document and spreadsheets downloaded February 2013 from website: http://www.kgs.ku.edu/mesaverde.

Clennell, M. B., 1997, Tortuosity: a guide through the maze: Geological Society, London, Special Publications v. 122; p. 299-344, doi:10.1144/GSL.SP.1997.122.01.18.

Clerke, E. A., 2009, Permeability, relative permeability, microscopic displacement efficiency, and pore geometry of M_1 bimodal pore systems in the Arab D limestone: SPE Journal, v. 14, #3, p. p 524-531.

Comisky , J. T., K. E. Newsham, J. A. Rushing, T. A. Blasingame, 2007, A comparative study of capillary-pressure-based empirical models for estimating absolute permeability in tight gas sands: 2007 SPE Annual Technical Conference and exhibition, Anaheim, CA, 11-14 November, 2007, SPE 110050, 18 p.

Dastidar, R., C. H. Sondergeld, and C. S. Rai, 2007, An improved empirical permeability estimator from mercury injection for tight clastic Rocks: Petrophysics, Vol. 48, No. 3, p. 186-187.

Erlich, R., E. L. Etris, D. Brumfield, L. P. Yuan, and S.J. Crabtree, 1991, Petrography and Reservoir Physics III: Physical Models for Permeability and Formation Factor: AAPG Bulletin, v. 75 #10, p. 1579 - 1592.

Huet, C. C., J. A. Rushing, K. E. Newsham, and T. A. Blasingame, 2005, A modified Purcell/Burdine model for estimating absolute permeability from mercury injection capillary pressure data: paper IPTC 10994 presented at the 2005 International Petroleum Technology Conference, Doha, Qatar, Nov. 21-23 2005.

Jones, F. O. and W. W. Owens, 1980, A laboratory study of low permeability gas sands: Journal of Petroleum Technology, September 1980, p. 1631-1640.

Kamath, J., 1992, Evaluation of Accuracy of Estimating Air Permeability from Mercury Injection Data: SPE Formation Evaluation, December, 1992 p. 304-310.

Katz, A. J. and A. H. Thompson, 1986, Quantitative prediction of permeability in porous rock: Physical Review Letters B, v. 34, #11, p. 8179-8181.

Katz, A. J. and A. H. Thompson, 1987, Prediction of rock electrical conductivity from mercury injection measurements: Journal of Geophysical Research B v 92, # B1, p. 599-607.

Kolodzie, S., 1980, Analysis of Pore Throat Size and Use of the Waxman-Smits Equation to Determine OOIP in Spindle Field, Colorado: 55th Annual Fall Technical Conference of Society of Petroleum Engineers, Sept. 21-24, 1980. paper SPE9382.

Lemorand, R., 2003, Interpretation of mercury injection curves to derive pore size distribution: Society of Core Analysts 2003 symposium, paper SCA2003-52. downloaded from http://www.scaweb.org/assets/papers/2003_papers/SCA2003-52.pdf, November 2013.

Ma, S-X. and N. R. Morrow, 1996, Relationships between porosity and permeability for porous rocks: 1996 International Symposium of the Society of Core Analysts, Sept. 8-10, Montpelier, France paper 9610, 12 p.

Pittman, E. D., 1992, Relation of porosity and permeability to various parameters derived from mercury injection capillary pressure curves for sandstone: AAPG Bulletin v. 76, #2, p. 191-198.

Purcell, W. R., 1949, Capillary pressures—their measurement using mercury and the calculation of permeability: Transaction AIME, v. 186, p. 39-48.

Swanson, B. F., 1981, A simple correlation between permeability and mercury capillary pressures: Journal of Petroleum Technology, December 1981, p. 2488 – 2504.

Thomeer, J. H. M., 1960, Introduction of a pore geometrical factor defined by the capillary pressure curve (AIME technical note 2057): Journal of Petroleum Technology, March 1960, p. 73 – 77.

Thomeer, J. H. M., 1983, Air permeability as a function of three pore-network parameters: Journal of Petroleum Technology, April 1983, p. 809 – 814.

Thomas, R. D. and D. C. Ward, 1972, Effect of overburden pressure and water saturation on gas permeability of tight sandstone cores: Journal of Petroleum Technology, v. 24, #2, February 1972, p. 120 – 124.

Walls, J. D. and J. O. Amaefule, 1985, Capillary Pressure and Permeability Relationships in Tight Gas Sands: 1985 SPE Low Permeability Gas Reservoir Conference, Denver, CO, May 19-22, 1985 Paper SPE13879.

Walls, J. D., A. M. Nur, and T. Bourbie, 1982, Effects of pressure and partial water saturation on gas permeability in tight sands: experimental results: Journal of Petroleum Technology, v. 34 #4, April, 1982, p. 930 – 936.

Acknowledgments

I thank Alan Byrnes for measuring the DOE data set and the US Department of Energy for funding that study and making the entire data set available to the public. This is one of the few public domain data sets where MICP methodology can be assessed and discussed in an open forum. I also thank Russell Davies and Rob Knipe for discussion of some preliminary ideas on MICP analysis of heterogeneous rocks that influenced the development of the methodologies presented here.

Presented at AAPG ANNUAL MEETING, Denver, 2015